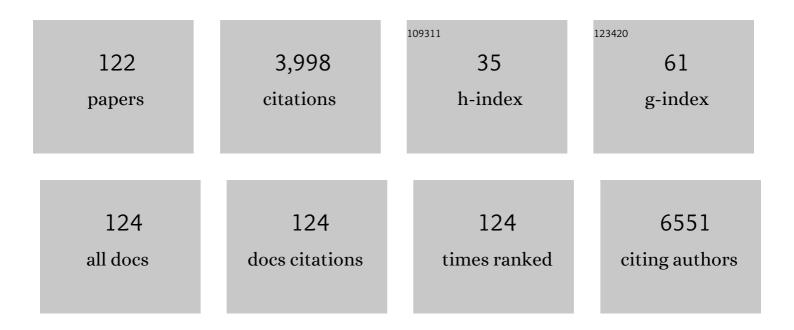
List of Publications by Year in descending order

Source: https://exaly.com/author-pdf/385555/publications.pdf Version: 2024-02-01



#	Article	IF	CITATIONS
1	Topological Insulator \$\$hbox {Bi}_{2}hbox {Se}_{3}\$\$ Films on Silicon Substrates. Journal of Electronic Materials, 2020, 49, 2191-2196.	2.2	5
2	Large-area periodic arrays of gold nanostars derived from HEPES-, DMF-, and ascorbic-acid-driven syntheses. Nanoscale, 2020, 12, 16489-16500.	5.6	23
3	Light Emitting Devices Based on Quantum Well-Dots. Applied Sciences (Switzerland), 2020, 10, 1038.	2.5	37
4	Gallium nitride tunneling field-effect transistors exploiting polarization fields. Applied Physics Letters, 2020, 116, .	3.3	7
5	Layered two-dimensional selenides and tellurides grown by molecular beam epitaxy. , 2020, , 235-269.		1
6	Plasmon-Mediated Synthesis of Periodic Arrays of Gold Nanoplates Using Substrate-Immobilized Seeds Lined with Planar Defects. Nano Letters, 2019, 19, 5653-5660.	9.1	50
7	Magnetotransport and superconductivity in InBi films grown on Si(111) by molecular beam epitaxy. Journal of Applied Physics, 2019, 126, 103901.	2.5	4
8	TEM Investigations of Ion-Irradiated Cerium Oxide Thin Film. Microscopy and Microanalysis, 2019, 25, 1620-1621.	0.4	0
9	Realization of GaN PolarMOS using selective-area regrowth by MBE and its breakdown mechanisms. Japanese Journal of Applied Physics, 2019, 58, SCCD15.	1.5	18
10	In-situ transmission electron microscopy determination of solid-state diffusion in the aluminum-nickel system. Journal of Solid State Chemistry, 2019, 276, 114-121.	2.9	15
11	Crystal Structure of Individual CsPbBr <sub>3</sub> Perovskite Nanocubes. Inorganic Chemistry, 2019, 58, 1555-1560.	4.0	61
12	Rotationally aligned hexagonal boron nitride on sapphire by high-temperature molecular beam epitaxy. Physical Review Materials, 2019, 3, .	2.4	25
13	Programmable bias field observed in graded ferromagnetic semiconductor films with broken symmetry. Physical Review Materials, 2019, 3, .	2.4	4
14	GaN/NbN epitaxial semiconductor/superconductor heterostructures. Nature, 2018, 555, 183-189.	27.8	116
15	Bimodality in Arrays of In0.4Ga0.6As Hybrid Quantum-Confined Heterostructures Grown on GaAs Substrates. Semiconductors, 2018, 52, 53-58.	0.5	6
16	Dependence of ferromagnetic properties on phosphorus concentration in Ga1-xMnxAs1-yPy. Journal of Vacuum Science and Technology B:Nanotechnology and Microelectronics, 2018, 36, 02D104.	1.2	7
17	Crystallization of a Mechanically Activated CuTi Alloy. Doklady Physics, 2018, 63, 45-49.	0.7	2
18	Room temperature microwave oscillations in GaN/AlN resonant tunneling diodes with peak current densities up to 220 kA/cm2. Applied Physics Letters, 2018, 112, .	3.3	51

#	Article	IF	CITATIONS
19	MBE growth of few-layer 2H-MoTe2 on 3D substrates. Journal of Crystal Growth, 2018, 482, 61-69.	1.5	43
20	Mesoporous metal - silica materials: Synthesis, catalytic and thermal properties. Microporous and Mesoporous Materials, 2018, 257, 175-184.	4.4	18
21	Light-Assisted Growth of Hexagonal Au Nanostructures on Sapphire Substrates. Microscopy and Microanalysis, 2018, 24, 1678-1679.	0.4	0
22	Kinetics and Mechanism of Ignition in Reactive Al/Ni Nanostructured Materials. Journal of Physical Chemistry C, 2018, 122, 27082-27092.	3.1	21
23	Tunable mesoporous films from copolymers with degradable side chains as membrane precursors. Journal of Membrane Science, 2018, 567, 104-114.	8.2	6
24	Orthogonal interfacial exchange coupling in GaMnAsP/GaMnAs bilayers. AIP Advances, 2018, 8, 056401.	1.3	4
25	Growth of yttrium iron garnet on SiO2. Journal of Vacuum Science and Technology A: Vacuum, Surfaces and Films, 2018, 36, .	2.1	1
26	Identifying the True Catalyst in the Reduction of 4-Nitrophenol: A Case Study Showing the Effect of Leaching and Oxidative Etching Using Ag Catalysts. ACS Catalysis, 2018, 8, 8879-8888.	11.2	43
27	In Situ TEM Study of Diffusion Kinetics in Al/Ni Nanomaterials. Microscopy and Microanalysis, 2018, 24, 1840-1841.	0.4	0
28	Structural transformations of highly porous nickel catalysts during ethanol conversion towards hydrogen. International Journal of Hydrogen Energy, 2018, 43, 13225-13236.	7.1	11
29	Structural evolution of dilute magnetic (Sn,Mn)Se films grown by molecular beam epitaxy. Journal of Applied Physics, 2017, 121, 075301.	2.5	5
30	MBE-grown 232–270 nm deep-UV LEDs using monolayer thin binary GaN/AlN quantum heterostructures. Applied Physics Letters, 2017, 110, .	3.3	105
31	Nuclear-blast induced nanotextures in quartz and zircon within Trinitite. American Mineralogist, 2017, 102, 445-460.	1.9	10
32	Light-emitting and photovoltaic devices based on quantum well-dots hybrid nanostructures. , 2017, , .		2
33	Electrochemical synthesis to convert a Ag film into Ag nanoflowers with high electrocatalytic activity. Chemical Communications, 2017, 53, 6752-6755.	4.1	33
34	Excitonic lasing of strain-free InP(As) quantum dots in AlInAs microdisk. Applied Physics Letters, 2017, 110, .	3.3	3
35	New Tunneling Features in Polar III-Nitride Resonant Tunneling Diodes. Physical Review X, 2017, 7, .	8.9	42
36	Deep-UV emission at 219 nm from ultrathin MBE GaN/AlN quantum heterostructures. Applied Physics Letters, 2017, 111, .	3.3	54

#	Article	IF	CITATIONS
37	Mobilization and agglomeration of uraninite nanoparticles: A nano-mineralogical study of samples from the Matoush Uranium ore deposit. American Mineralogist, 2017, 102, 1776-1787.	1.9	7
38	Origin of the Size-Dependent Stokes Shift in CsPbBr <sub>3</sub> Perovskite Nanocrystals. Journal of the American Chemical Society, 2017, 139, 12201-12208.	13.7	240
39	Combustion Synthesis of Ni-SiO2 Nanoscale Materials. Microscopy and Microanalysis, 2017, 23, 1866-1867.	0.4	Ο
40	Molecular beam epitaxy growth and structure of self-assembled Bi <sub>2</sub> Se <sub>3</sub> /Bi <sub>2</sub> MnSe <sub>4</sub> multilayer heterostructures. New Journal of Physics, 2017, 19, 085002.	2.9	58
41	Optical properties of hybrid quantum-well–dots nanostructures grown by MOCVD. Semiconductors, 2017, 51, 357-362.	0.5	2
42	AlGaN Nanostructures with Extremely High Room-Temperature Internal Quantum Efficiency of Emission Below 300Anm. Journal of Electronic Materials, 2017, 46, 3888-3893.	2.2	3
43	High-temperature p-type polarization doped AlGaN cladding for sub-250 nm deep-UV quantum well LEDs by MBE. , 2017, , .		Ο
44	Room temperature weak ferromagnetism in Sn1â^'xMnxSe2 2D films grown by molecular beam epitaxy. APL Materials, 2016, 4, .	5.1	28
45	Experimental demonstration of single electron transistors featuring SiO2 plasma-enhanced atomic layer deposition in Ni-SiO2-Ni tunnel junctions. Journal of Vacuum Science and Technology A: Vacuum, Surfaces and Films, 2016, 34, .	2.1	5
46	Large area growth of layered WSe <sub>2</sub> films. Semiconductor Science and Technology, 2016, 31, 095002.	2.0	34
47	Ga–In intermixing, intrinsic doping, and Wigner localization in the emission spectra of self-organized InP/GaInP quantum dots. Journal Physics D: Applied Physics, 2016, 49, 475301.	2.8	17
48	High-quality InN films on GaN using graded InGaN buffers by MBE. Japanese Journal of Applied Physics, 2016, 55, 05FD12.	1.5	16
49	Sub-230 nm deep-UV emission from GaN quantum disks in AlN grown by a modified Stranski–Krastanov mode. Japanese Journal of Applied Physics, 2016, 55, 05FF06.	1.5	25
50	Transforming Layered to Nonlayered Two-Dimensional Materials: Cation Exchange of SnS <sub>2</sub> to Cu <sub>2</sub> SnS <sub>3</sub> . ACS Energy Letters, 2016, 1, 175-181.	17.4	19
51	Silicon carbide ceramics: Mechanical activation, combustion and spark plasma sintering. Ceramics International, 2016, 42, 12686-12693.	4.8	34
52	Optical properties of hybrid quantum-confined structures with high absorbance. Semiconductors, 2016, 50, 1180-1185.	0.5	2
53	Controllable growth of layered selenide and telluride heterostructures and superlattices using molecular beam epitaxy. Journal of Materials Research, 2016, 31, 900-910.	2.6	85
54	Effect of alloying on elastic properties of ternary Ni-Al-Ti system: Experimental validation. Journal of Alloys and Compounds, 2016, 688, 534-541.	5.5	7

#	Article	IF	CITATIONS
55	Origin of Spontaneous Core–Shell AlGaAs Nanowires Grown by Molecular Beam Epitaxy. Crystal Growth and Design, 2016, 16, 7251-7255.	3.0	42
56	Layered transition metal dichalcogenides: promising near-lattice-matched substrates for GaN growth. Scientific Reports, 2016, 6, 23708.	3.3	76
57	First demonstration of strained AlN/GaN/AlN quantum well FETs on SiC. , 2016, , .		4
58	Atomic layer deposition of Al2O3 for single electron transistors utilizing Pt oxidation and reduction. Journal of Vacuum Science and Technology A: Vacuum, Surfaces and Films, 2016, 34, .	2.1	7
59	Spray Solution Combustion Synthesis of Metallic Hollow Microspheres. Journal of Physical Chemistry C, 2016, 120, 7165-7171.	3.1	30
60	Combustion in reactive multilayer Ni/Al nanofoils: Experiments and molecular dynamic simulation. Combustion and Flame, 2016, 166, 158-169.	5.2	73
61	Exothermic Self-Sustained Waves with Amorphous Nickel. Journal of Physical Chemistry C, 2016, 120, 5827-5838.	3.1	23
62	Growth of multiple WS <sub>2</sub> /SnS layered semiconductor heterojunctions. Nanoscale, 2016, 8, 2143-2148.	5.6	51
63	Solid-flame: Experimental validation. Combustion and Flame, 2016, 163, 487-493.	5.2	36
64	Structural and optical properties of PA MBE AlGaN quantum well heterostructures grown on c-Al2O3 by using flux- and temperature-modulated techniques. Journal of Materials Research, 2015, 30, 2871-2880.	2.6	17
65	TEM Analysis of Structural Transformation in Al/Ni Nanomaterials under High Energy Ion Irradiation. Microscopy and Microanalysis, 2015, 21, 583-584.	0.4	Ο
66	TEM Analysis of Defects in AlGaN Heterostructures Grown on C-Al2O3 by Plasma Assisted Molecular Beam Epitaxy. Microscopy and Microanalysis, 2015, 21, 1803-1804.	0.4	0
67	High temperature laser diode based on a single sheet of quantum dots. Semiconductor Science and Technology, 2015, 30, 105005.	2.0	1
68	Hybrid InGaAs quantum well–dots nanostructures for light-emitting and photo-voltaic applications. Nanotechnology, 2015, 26, 385202.	2.6	39
69	Effect of the bimodality of a QD array on the optical properties and threshold characteristics of QD lasers. Semiconductors, 2015, 49, 1090-1094.	0.5	11
70	Low temperature AlN growth by MBE and its application in HEMTs. Journal of Crystal Growth, 2015, 425, 133-137.	1.5	23
71	Nickel Oxide Reduction by Hydrogen: Kinetics and Structural Transformations. Journal of Physical Chemistry C, 2015, 119, 16131-16138.	3.1	92
72	Irradiation-Enhanced Reactivity of Multilayer Al/Ni Nanomaterials. ACS Applied Materials & Interfaces, 2015, 7, 11272-11279.	8.0	33

SERGEI ROUVIMOV

#	Article	IF	CITATIONS
73	Defect engineering in AlGaN-based UV optoelectronic heterostructures grown on c-Al2O3 by plasma-assisted molecular beam epitaxy. Materials Research Society Symposia Proceedings, 2015, 1741, 47.	0.1	1
74	Comprehensive structural and optical characterization of MBE grown MoSe <sub>2</sub> on graphite, CaF <sub>2</sub> and graphene. 2D Materials, 2015, 2, 024007.	4.4	120
75	Highly stable Ni–Al2O3 catalyst prepared from a Ni–Al layered double hydroxide for ethanol decomposition toward hydrogen. Applied Catalysis A: General, 2015, 508, 37-44.	4.3	32
76	GaAs quantum wellâ€dots solar cells with spectral response extended to 1100Ânm. Electronics Letters, 2015, 51, 1602-1604.	1.0	37
77	Deep-UV LEDs using polarization-induced doping: Electroluminescence at cryogenic temperatures. , 2015, , .		1
78	Low temperature decomposition of hydrous hydrazine over FeNi/Cu nanoparticles. Applied Catalysis A: General, 2014, 476, 47-53.	4.3	94
79	Structure evolution and reaction mechanism in the Ni/Al reactive multilayer nanofoils. Acta Materialia, 2014, 66, 86-96.	7.9	87
80	In Situ Preparation of Highly Stable Ni-Based Supported Catalysts by Solution Combustion Synthesis. Journal of Physical Chemistry C, 2014, 118, 26191-26198.	3.1	58
81	Bulk Cu–Cr nanocomposites by high-energy ball milling and spark plasma sintering. Journal of Alloys and Compounds, 2014, 617, 39-46.	5.5	56
82	Ultrasmall α-Fe <sub>2</sub> O <sub>3</sub> Superparamagnetic Nanoparticles with High Magnetization Prepared by Template-Assisted Combustion Process. Journal of Physical Chemistry C, 2014, 118, 16264-16271.	3.1	104
83	High-voltage field effect transistors with wide-bandgap <i>β</i> -Ga2O3 nanomembranes. Applied Physics Letters, 2014, 104, .	3.3	288
84	Fine Structural Studies of AlGaN Laser Heterostructures with Digitally Alloyed Quantum Wells Grown on c-Al2O3 by plasma-Assisted Molecular Beam Epitaxy. Microscopy and Microanalysis, 2014, 20, 80-81.	0.4	0
85	Atomic Structure of Thin MoSe2 Films Grown by Molecular Beam Epitaxy. Microscopy and Microanalysis, 2014, 20, 164-165.	0.4	19
86	TEM/STEM Analysis of NiO Reduction to Ni during Annealing in H2 Atmosphere. Microscopy and Microanalysis, 2014, 20, 1898-1899.	0.4	0
87	Combustion synthesis of graphene materials. Carbon, 2013, 62, 302-311.	10.3	36
88	Highly selective bimetallic FeMoP catalyst for C–O bond cleavage of aryl ethers. Journal of Catalysis, 2013, 305, 256-263.	6.2	127
89	Solution Combustion Synthesis of Nano-Crystalline Metallic Materials: Mechanistic Studies. Journal of Physical Chemistry C, 2013, 117, 24417-24427.	3.1	170
90	Influence of the high energy ball milling on structure and reactivity of the Ni+Al powder mixture. Journal of Alloys and Compounds, 2013, 577, 600-605.	5.5	75

#	Article	IF	CITATIONS
91	Catalytic Performance and in Situ Surface Chemistry of Pure α-MnO <sub>2</sub> Nanorods in Selective Reduction of NO and N <sub>2</sub> O with CO. Journal of Physical Chemistry C, 2013, 117, 8329-8335.	3.1	66
92	Formation of Three-Dimensional Islands in Subcritical Layer Deposition in Stranski-Krastanow Growth. Physical Review Letters, 2013, 110, 176101.	7.8	7
93	Nanomembrane β-Ga <inf>2</inf> O <inf>3</inf> high-voltage field effect transistors. , 2013, , .		1
94	W and two-dimensional WO <sub>3</sub> /W nanocrystals produced by controlled self-sustaining reduction of sodium tungstate. Journal of Materials Research, 2013, 28, 2611-2621.	2.6	5
95	Microstructure-reactivity relationship of Ti + C reactive nanomaterials. Journal of Applied Physics, 2013, 113, 024302.	2.5	27
96	Controlling Sizeâ€Induced Phase Transformations Using Chemically Designed Nanolaminates. Angewandte Chemie - International Edition, 2013, 52, 13211-13214.	13.8	33
97	Crystallite Thickness Estimates from Precession Electron Diffraction Patterns for Structural Fingerprinting in the Quasi-kinematic Limit. Microscopy and Microanalysis, 2012, 18, 562-563.	0.4	1
98	Aberration-corrected High Resolution Transmission Electron Microscopy of [(SnSe)]m[MoSe2]n films. Microscopy and Microanalysis, 2012, 18, 1630-1631.	0.4	0
99	Introduction to the special issue: In memoriam Professor Gertrude Fleming Rempfer on the occasion of her 100th birthday. Ultramicroscopy, 2012, 119, 1-4.	1.9	0
100	New Layered Intergrowths in the Sn-Mo-Se System. Journal of Electronic Materials, 2012, 41, 1476-1480.	2.2	27
101	Rattler-seeded InSb nanoinclusions from metastable indium-filled In0.1Co4Sb12 skutterudites for high-performance thermoelectrics. Acta Materialia, 2012, 60, 2178-2185.	7.9	43
102	Structural investigations of ferecrystals [(SnSe) <inf>1+δ</inf> ] <inf>m</inf> [TSe <inf>2</inf> ] <inf>n&amp;l (T = Mo, Ta) by means of transmission electron microscopy. , 2011, , .</inf>	lt;/inf>	2
103	Precession electron diffraction & automated crystallite orientation/phase mapping in a transmission electron microscope. , 2011, , .		1
104	Automated Crystallite Orientation and Phase Mapping in a Transmission Electron Microscope. Materials Research Society Symposia Proceedings, 2011, 1318, 1.	0.1	0
105	Thermoelectric properties of indium-filled InxRh4Sb12 skutterudites. Journal of Alloys and Compounds, 2011, 509, 6289-6295.	5.5	16
106	Structure analysis of CVD graphene films based on HRTEM contrast simulations. Physica Status Solidi (A) Applications and Materials Science, 2011, 208, 2681-2687.	1.8	4
107	High spatial resolution semiâ€automatic crystallite orientation and phase mapping of nanocrystals in transmission electron microscopes. Crystal Research and Technology, 2011, 46, 589-606.	1.3	118
108	Effect of annealing on ZnO nanowires grown at low temperature. , 2011, , .		0

SERGEI ROUVIMOV

#	Article	IF	CITATIONS
109	Structure analysis of CVD graphene films based on HRTEM contrast simulations. , 2011, , .		4
110	Nano-materials for Renewable Energy: Toward the integration of education with research and internship. , 2011, , .		0
111	Automated nanocrystal orientation and phase mapping in the transmission electron microscope on the basis of precession electron diffraction. Zeitschrift FÃ1⁄4r Kristallographie, 2010, 225, 103-109.	1.1	269
112	Precession electron diffraction and its advantages for structural fingerprinting in the transmission electron microscope. Zeitschrift Für Kristallographie, 2010, 225, 110-124.	1.1	15
113	Structural Fingerprinting of Nanocrystals: Advantages of Precession Electron Diffraction, Automated Crystallite Orientation and Phase Maps. Materials Research Society Symposia Proceedings, 2009, 1184, 1.	0.1	8
114	Precession electron diffraction and its utility for structural fingerprinting in the transmission electron microscope. , 2009, , .		1
115	Automated crystal phase and orientation mapping of nanocrystals in a transmission electron microscope. , 2009, , .		0
116	Structural Fingerprinting of Nanocrystals in the Transmission Electron Microscope. Microscopy and Microanalysis, 2009, 15, 1230-1231.	0.4	0
117	High Throughput Automated Crystal Orientation and Phase Mapping of Nanoparticles from HREM - TEM Images. Microscopy and Microanalysis, 2009, 15, 756-757.	0.4	5
118	Determining Projected Symmetries for Structural Fingerprinting of Nanocrystals. Microscopy and Microanalysis, 2009, 15, 776-777.	0.4	0
119	Surface recombination velocity of silicon wafers by photoluminescence. Applied Physics Letters, 2005, 86, 112110.	3.3	39
120	Photoluminescence Intensity Analysis in Application to Contactless Characterization of Silicon Wafers. Journal of the Electrochemical Society, 2003, 150, G436.	2.9	16
121	Methods of Electron Crystallography as Tools for Materials Analysis. Solid State Phenomena, 0, 186, 1-6.	0.3	1
122	Monolayerâ€Range Compositional Modulations in Al x Ga 1â^' x N ( x  = 0.6–0.75) Layers Grown Using Plasmaâ€Assisted Molecular Beam Epitaxy under Meâ€Rich Conditions with an Offâ€Centered Spatial Distribution of Activated Nitrogen Flux. Physica Status Solidi (A) Applications and Materials Science, 0, , 2100550.	1.8	1